

AD-A124 583

AN ASSESSMENT OF FACTORS AFFECTING PREDICTION OF
NEAR-FIELD DEVELOPMENT O. (U) COMPUTATIONAL MECHANICS
CONSULTANTS INC KNOXVILLE TN A J BAKER ET AL. JUN 82

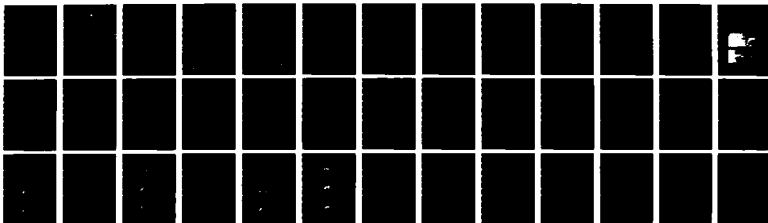
1/1

UNCLASSIFIED

NADC-81177-68 N62269-81-C-0395

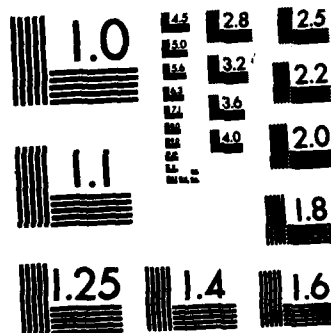
F/G 1/3

NL



END

FILMED
+
DTIC



MICROCOPY RESOLUTION TEST CHART
NATIONAL BUREAU OF STANDARDS-1963-A

12



ADA 124583

**AN ASSESSMENT OF FACTORS AFFECTING
PREDICTION OF NEAR-FIELD DEVELOPMENT
OF A SUBSONIC VSTOL JET IN CROSS-FLOW**

**A.J. Baker and J.A. Orzechowski
Computational Mechanics Consultants, Inc.
3601-A Chapman Highway
Knoxville, TN 37920**

JUNE 1982

**FINAL REPORT
CONTRACT NO. N62269-81C-0395**

**DTIC
REGISTERED
FEB 17 1983
H**

Approved for Public Release; Distribution Unlimited

**Prepared For
C. Henderson (Code 6053)
Aircraft and Crew Systems Technology Directorate
NAVAL AIR DEVELOPMENT CENTER
Warminster, PA 18974**

DTIC FILE COPY

83 00 017 002

NADC-81177-60


N O T I C E S

REPORT NUMBERING SYSTEM - The numbering of technical project reports issued by the Naval Air Development Center is arranged for specific identification purposes. Each number consists of the Center acronym, the calendar year in which the number was assigned, the sequence number of the report within the specific calendar year, and the official 2-digit correspondence code of the Command Office or the Functional Directorate responsible for the report. For example: Report No. NADC-78015-20 indicates the fifteenth Center report for the year 1978, and prepared by the Systems Directorate. The numerical codes are as follows:

| CODE | OFFICE OR DIRECTORATE |
|------|---|
| 00 | Commander, Naval Air Development Center |
| 01 | Technical Director, Naval Air Development Center |
| 02 | Comptroller |
| 10 | Directorate Command Projects |
| 20 | Systems Directorate |
| 30 | Sensors & Avionics Technology Directorate |
| 40 | Communication & Navigation Technology Directorate |
| 50 | Software Computer Directorate |
| 60 | Aircraft & Crew Systems Technology Directorate |
| 70 | Planning Assessment Resources |
| 80 | Engineering Support Group |

PRODUCT ENDORSEMENT - The discussion or instructions concerning commercial products herein do not constitute an endorsement by the Government nor do they convey or imply the license or right to use such products.

APPROVED BY:


T. J. GALLAGHER
CAPT, MSC, USN

DATE:

24 Jan 1983

| REPORT DOCUMENTATION PAGE | | READ INSTRUCTIONS BEFORE COMPLETING FORM |
|--|-------------------------------------|--|
| 1. REPORT NUMBER NADC-81177-80 | 2. GOVT ACCESSION NO. AD-A124583 | 3. RECIPIENT'S CATALOG NUMBER |
| 4. TITLE (and Subtitle) AN ASSESSMENT OF FACTORS AFFECTING PREDICTION OF NEAR-FIELD DEVELOPMENT OF A SUBSONIC VSTOL JET IN CROSS-FLOW. | | 5. TYPE OF REPORT & PERIOD COVERED FINAL REPORT 9/81-6/82 |
| | | 6. PERFORMING ORG. REPORT NUMBER |
| 7. AUTHOR(s) A.J. BAKER and J.A. ORZECOWSKI | | 8. CONTRACT OR GRANT NUMBER(s) N62269-81C-0395 |
| 9. PERFORMING ORGANIZATION NAME AND ADDRESS COMPUTATIONAL MECHANICS CONSULTANTS, INC. 3601-A Chapman Highway Knoxville, TN 37920 | | 10. PROGRAM ELEMENT, PROJECT, TASK AREA & WORK UNIT NUMBERS |
| 11. CONTROLLING OFFICE NAME AND ADDRESS C. Henderson (Code 6053) Aircraft and Crew System Technology Directorate Naval Air Development Center, Warminster, PA 18974 | | 12. REPORT DATE June 1982 |
| | | 13. NUMBER OF PAGES 36 |
| 14. MONITORING AGENCY NAME & ADDRESS (if different from Controlling Office) | | 15. SECURITY CLASS. (of this report) UNCLASSIFIED |
| | | 15a. DECLASSIFICATION/DOWNGRADING SCHEDULE |
| 16. DISTRIBUTION STATEMENT (of this Report) Approved for Public Release; Distribution Unlimited. | | |
| 17. DISTRIBUTION STATEMENT (of the abstract entered in Block 20, if different from Report) | | |
| 18. SUPPLEMENTARY NOTES | | |
| 19. KEY WORDS (Continue on reverse side if necessary and identify by block number) VSTOL Jet Three-Dimensional Crossflow Turbulent Flow Numerical Solutions | | |
| 20. ABSTRACT (Continue on reverse side if necessary and identify by block number) A three-dimensional parabolic Navier-Stokes numerical solution algorithm has been analyzed for prediction of the nearfield flow development of a VSTOL jet in subsonic crossflow. The essential aspects of algorithm definition, with regards to initial and boundary condition specifications, has been summarized. A momentum conserving pressure gradient computation has been developed to complete the problem definition and facilitate problem initialization. A sequence of overlapping interaction solutions has been evaluated for prediction of a circular jet at $\lambda = 8.0$. The results of the 3DPNS predictions have compared qualitatively with the sparse available experimental data. It is crucial that quality data be acquired to permit quantitative assessment of the results of this analysis procedure. | | |

PREFACE

The effort reported herein was performed by Computational Mechanics Consultants, Inc. during the period October 1981 through June, 1982, with Dr. A. J. Baker as Principal Investigator. The sponsorship was provided by the Naval Air Development Center, Warminster, Pennsylvania, under Contract No. N62269-81C-0395. The NADC Technical Monitor was Mr. Campbell C. Henderson.

| | | |
|------------------------------|--------------|--|
| Accession For | | <input checked="checked" type="checkbox"/> |
| NTIS GRA&I | | <input type="checkbox"/> |
| DTIC TAB | | <input type="checkbox"/> |
| Unannounced Justification | | |
| By _____ | | |
| Distribution/ | | |
| Availability Codes | | |
| Dist | Avail and/or | Special |
| A | | |

0110
1000
2

TABLE OF CONTENTS

| | |
|---|--------|
| PREFACE | iii |
| TABLE OF CONTENTS | iv |
| LIST OF SYMBOLS | v |
| LIST OF FIGURES | viii |
| INTRODUCTION | 1 |
| THEORETICAL MODEL | 6 |
| Three-Dimensional Parabolic Navier-Stokes Equations | 6 |
| Reynolds Stress Closure Model For 3DPNS | 9 |
| Finite Element Solution Algorithm | 10 |
| DISCUSSION AND RESULTS | 13 |
| Problem Specification | 13 |
| Algorithm Specification | 15 |
| Circular Jet Analysis | 17 |
| SUMMARY & CONCLUSIONS | 25 |
| REFERENCES | 28 |
| DISTRIBUTION LIST | 30 |

LIST OF SYMBOLS

| | |
|----------------------|--|
| a | boundary condition coefficient |
| C | coefficient |
| d | differential |
| D | jet diameter |
| e | finite element index |
| E | mean flow strain rate tensor |
| f | function of known argument |
| h | integration step size |
| k | turbulence kinetic energy; interpolation polynomial degree |
| \mathcal{L} | differential operator; length scale |
| L | differential operator |
| M | number of finite elements spanning R^n |
| n | unit normal vector; dimensionality |
| N | finite element cardinal basis |
| p | pressure; iteration index |
| q | generalized dependent variable |
| Q | generalized discretized dependent variable |
| R | domain of elliptic operator |
| Re | Reynolds number |
| S | finite element assembly operator |
| u_i | mean flow velocity vector |
| $\overline{u_i u_j}$ | Reynolds stress tensor |
| U | reference velocity |
| x_i | Cartesian coordinate system |
| α | parameter |
| ∂R | boundary of solution domain R^n |

| | |
|---------------|--|
| δ | Kronecker delta; increment |
| Δ | increment; element measure |
| ϵ | turbulence dissipation function |
| λ | jet velocity ratio |
| ν | kinematic viscosity |
| ρ | density |
| σ_{ij} | mean flow Stokes stress tensor |
| ϕ | harmonic function for conservation of mass |
| Ω | global solution domain |

Superscripts:

| | |
|---------------|--|
| h | approximation |
| n | dimension of R |
| o | initial condition |
| T | matrix transpose |
| $-$ | mass-weighted time-average |
| — | time average |
| $\hat{\cdot}$ | unit vector |
| \cdot | fluctuating component; ordinary derivative |

Subscripts:

| | |
|--------------|--------------------------------|
| ∞ | freestream reference condition |
| e | finite element domain |
| i, j, k, l | tensor indices |
| j | jet reference |
| n | normal |

Notation:

| | |
|------------|----------------|
| $\{ \}$ | column matrix |
| $[]$ | square matrix |
| \cup | union |
| \cap | intersection |
| ϵ | belongs to |
| $ $ | absolute value |

LIST OF FIGURES

| <u>Figure No.</u> | <u>Title</u> | <u>Page</u> |
|-------------------|---|-------------|
| 1. | Schematic Description for a VSTOL Jet in a Cross-Flow. | 2 |
| 2. | Oil Flow Streaklines on the Injection Plate, from McMahon and Mosher [8]. | 2 |
| | a) Blockage due to Solid Cylinder | |
| | b) Blockage due to Circular Cross-Section VSTOL Jet, $\lambda = 8$. | |
| 3. | Oil Flow Streaklines for a Circular VSTOL Jet, from Margason and Fearn [9]. | 3 |
| 4. | Experimental Velocity Distributions, Circular Cross-Section Jet, $\lambda = 8$, from Kamotani and Greber [10]. | 3 |
| | a) Axial Isovels, $X_1/D = 7.0$ | |
| | b) Transverse Plane Velocity Distribution, $X_1/D = 23$ | |
| 5. | Similitude for Circular Jet Centerline Trajectory, from Fearn and Weston [11]. | 4 |
| 6. | Experimental Measurement of VSTOL Jet Velocity Distributions, $Z/D = 1.0$ and $Z/D = 3.0$, $Y/D = 0.$, from Fearn and Benson [12]. | 4 |
| 7. | Experimental Measurement of VSTOL Jet Transverse Plane | 5 |
| 8. | 3DPNS Computational Simulation Solution Domain | 14 |
| | a) 3DPNS Solution Domain Ω | |
| | b) Transverse Solution Domain Discretization UR_e^2 | |
| 9. | Comparison of 3DPNS Virtual Region Solution, Transverse Velocity Distributions, Circular Cross-Section VSTOL Jet, $\lambda = 8.$, $X_1/D = 0.25$. | 18 |
| | a) $d\bar{p}/dx = 0$, Equation 27 | |
| | b) $d\bar{p}/dx \neq 0$, Equation 27 | |
| | c) $d\bar{p}/dx = 0$ and $\tilde{u}_2(c) = 0$ | |

| Figure No. | Title | Page |
|------------|--|------|
| 10. | Summary of 3DPNS Virtual Region Solution, Transverse Velocity Distributions, $\bar{u}_2 \equiv 0$ on Symmetry Plane, Circular Cross-Section VSTOL Jet, $\lambda = 8$. | 20 |
| | a) $X_1/D = 0.5$ | |
| | b) $X_1/D = 0.75$ | |
| | c) $X_1/D = 1.0$ | |
| 11. | Summary of First Interaction Solution Transverse Plane Velocity Distributions, Circular Cross-Section VSTOL Jet, $\lambda = 8$. | 22 |
| | a) $X_1/D = 0.5$ | |
| | b) $X_1/D = 0.75$ | |
| | c) $X_1/D = 1.0$ | |
| 12. | Summary of Second Interaction Solution Transverse Plane Velocity Distributions, Circular Cross-Section VSTOL Jet, $\lambda = 8$. | 23 |
| 13. | Second Interaction Solution Fields, Circular Cross-Section VSTOL Jet, $\lambda = 8$, $X_1/D = 0.75$. | 24 |
| | a) Pressure Coefficient C_p . | |
| | b) Axial Velocity \bar{u}_1 | |
| 14. | Second Interaction Solution Reynolds Normal Stress Distributions, Circular Cross-Section VSTOL Jet, $\lambda = 8$, $X_1/D = 0.75$. | 26 |
| | a) Axial Normal Stress $\overline{u_1 u_1}$ | |
| | b) Transverse Normal Stress $\overline{u_2 u_2}$ | |
| | c) Transverse Normal Stress $\overline{u_3 u_3}$ | |
| 15. | Second Interaction Solution Reynolds Shear Stress Distributions, Circular Cross-Section VSTOL Jet, $\lambda = 8$, $X_1/D = 0.75$. | 27 |
| | a) Reynolds Shear Stress $\overline{u_1 u_2}$ | |
| | b) Reynolds Shear Stress $\overline{u_1 u_3}$ | |
| | c) Reynolds Shear Stress $\overline{u_2 u_3}$ | |

INTRODUCTION

Analysis and experimental evaluation of the aerodynamics of a subsonic VSTOL jet in cross-flow has been a major focus of a segment of the technical community, cf., references [1-7]. Figure 1 is a schematic illustration of the basic geometry. The fundamental differences in the cross-flow velocity field immediately adjacent to plane of injection of the VSTOL jet, $Z = 0$ in Figure 1, and a solid cylinder of the same diameter, is evident in the oil-flow streakline data of McMahan and Mosher [8], see Figure 2. Figure 3, a close-up view of similar data obtained at O.N.E.R.A., and referenced by Margason and Fearn [9], clearly illustrates an entrainment mechanism on the wake side of the jet, with the indication of localized reversal of the cross-flow velocity component. In the farfield, well downstream of the plane $Z = 0$, and referenced in the curvilinear coordinate system X_1 , Figure 1, the characteristic "horseshoe" isovel distribution for u_1 and secondary vortex structure for u_2 and u_3 is well documented. Figure 4 summarizes the data of Kamotani and Greber [10], as a typical example.

Much less is known regarding the interaction between the jet and the cross-flow in the nearfield, i.e., in the region $0 < Z/D < 2.0$. Fearn and Weston's [11] correlation of experimental data on the trajectory of the jet centerline. Figure 5, confirms the absence of data on $Z/D < 10$. Fearn et.al. [12] recently report a compilation of limited data, for circular cross-section VSTOL jets at $\lambda = 4$ and $\lambda = 8$, as obtained using a pitot-static pressure rake on the region $1.0 \leq Z/D \leq 3.0$. Figure 6 summarizes the measurement of the velocity component roughly parallel to the Z axis at $Z/D = 1.0$ and $Z/D = 3.0$. These data indicate some entrainment from the wake at $Z/D = 3.0$, but none is evident in the data at $Z/D = 1.0$. Figure 7 contains measured velocity vector distributions in the X - Y plane at the same Z/D stations. Neither wake entrainment nor secondary vortex structure is indicated at $Z/D = 1.0$. Limited entrainment is evident at $Z/D = 3.0$, but the data is too sparse to confirm that the secondary vortex has been initiated.

The purpose of this study was to expand and refine the three-dimensional parabolic Navier-Stokes algorithm, reported by Baker, et.al. [13], and to assess factors controlling prediction of the near-field flow development of a VSTOL jet in cross-flow at $\lambda = 8$. The results of this study are reported herein.

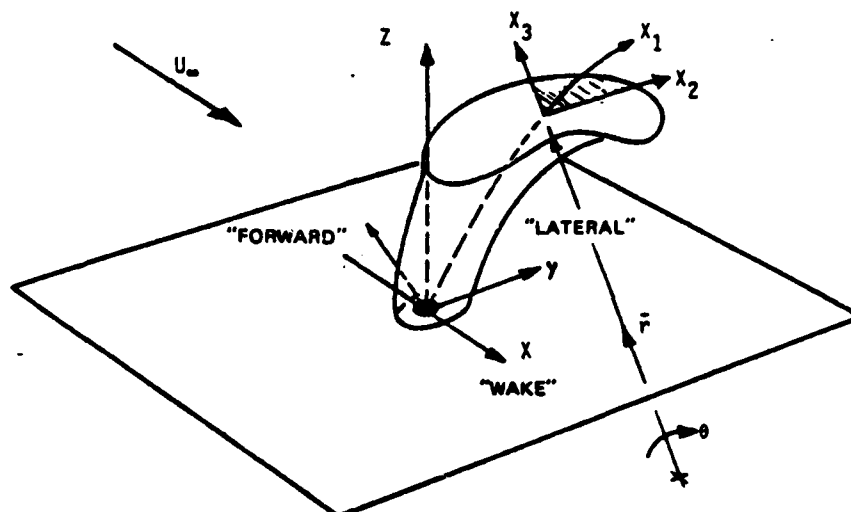
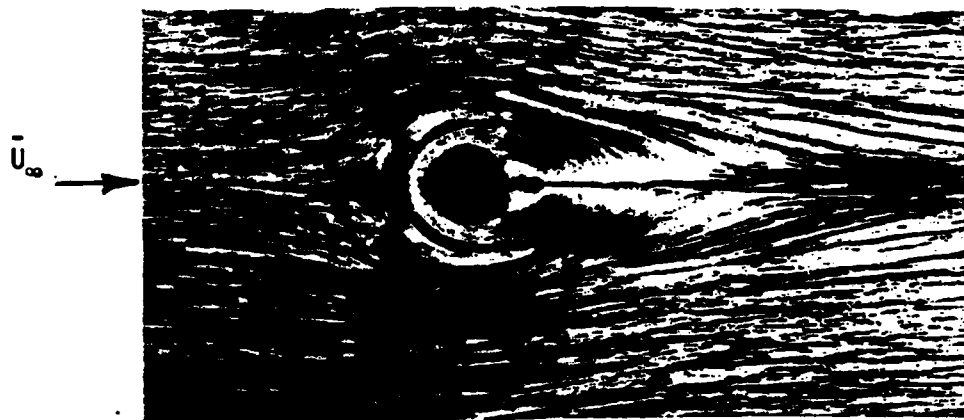
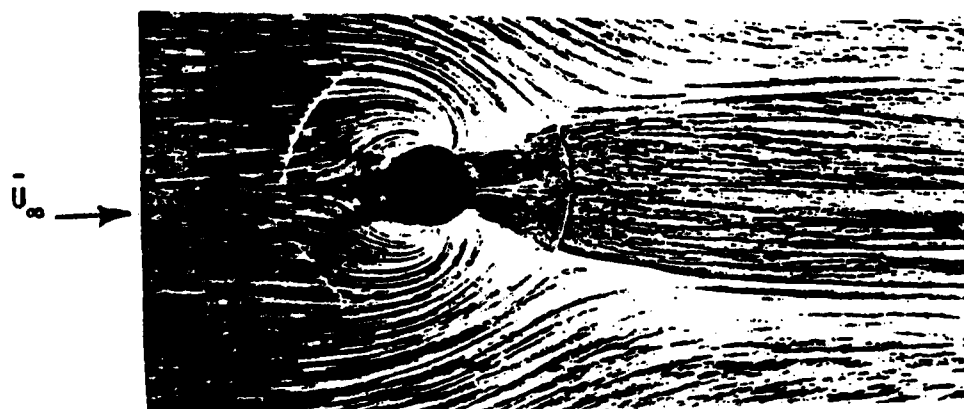


Figure 1. Schematic Description for a VSTOL Jet in a Cross-Flow.



a) Blockage due to Solid Cylinder



b) Blockage due to Circular Cross-Section VSTOL Jet, $\lambda = 8$.

Figure 2. Oil Flow Streaklines on the Injection Plate, from McMahon and Mosher [8].

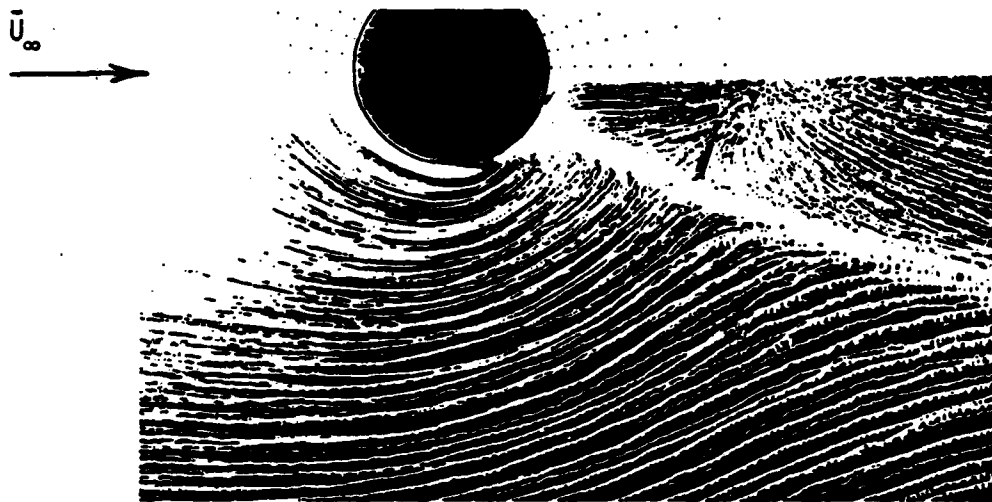
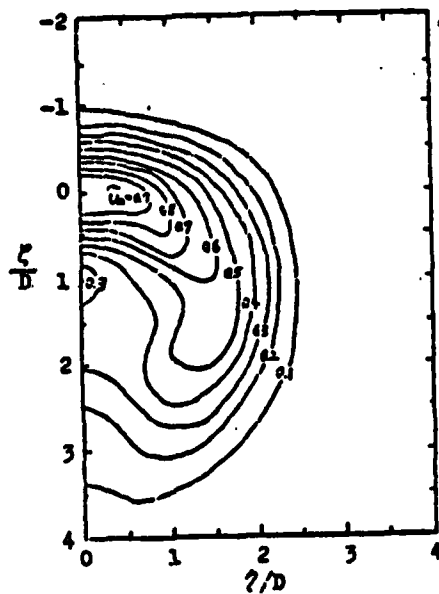
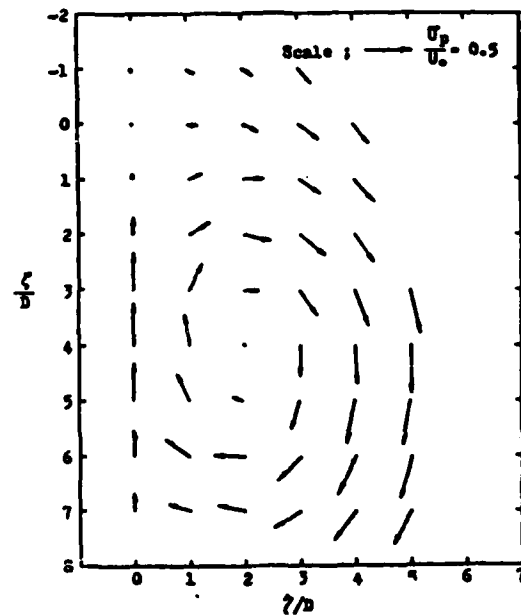


Figure 3. Oil Flow Streaklines For A Circular VSTOL Jet,
From Margason And Fearn [9].



a) Axial Isovels, $X_1/D = 7.0$



b) Transverse Plane Velocity
Distribution, $X_1/D = 23$

Figure 4. Experimental Velocity Distributions, Circular Cross-Section Jet,
 $\lambda = 8$, from Kamotani and Greber [10].

4

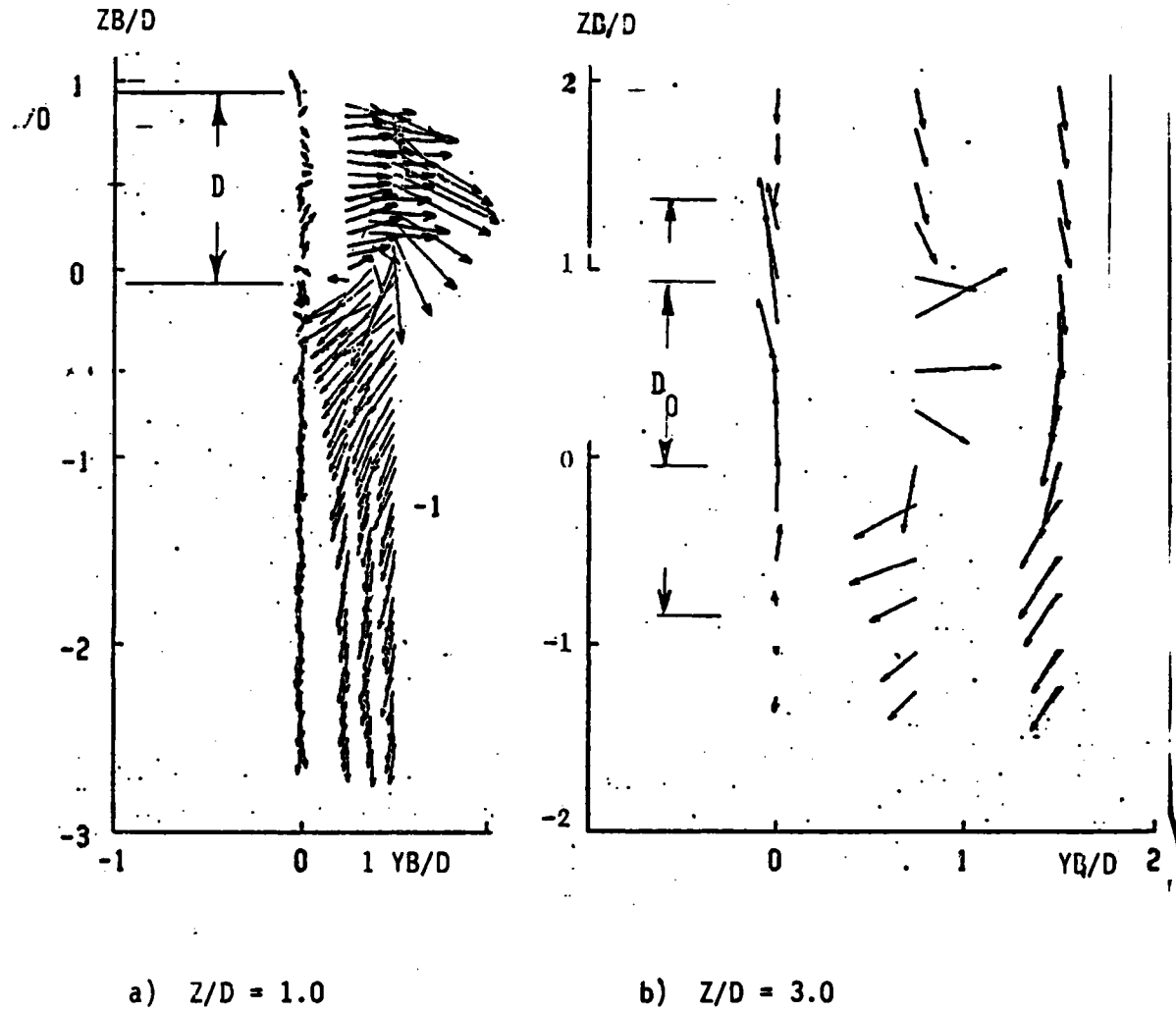


Figure 7. Experimental Measurement of VSTOL Jet Transverse Plane Velocity Distributions, from Fearn and Benson [12].

THEORETICAL MODEL

Three-Dimensional Parabolic Navier-Stokes Equations

The 3DPNS equation set is a simplification of the steady, three-dimensional time-averaged Navier-Stokes equations. In Cartesian tensor notation and employing superscript tilde and bar to denote mass-weighted and conventional time-averaging, respectively [14], the conservation equation form for an isoenergetic fluid is

$$L(\bar{\rho}) = \frac{\partial}{\partial x_j} [\bar{\rho} u_j] = 0 \quad (1)$$

$$L(\bar{\rho} \tilde{u}_i) = \frac{\partial}{\partial x_j} [\bar{\rho} \tilde{u}_i u_j + \bar{p} \delta_{ij} + \overline{\rho u_i u_j} - \bar{\sigma}_{ij}] = 0 \quad (2)$$

$$L(\bar{\rho} k) = \frac{\partial}{\partial x_j} \left[\bar{\rho} \tilde{u}_j k + (c_k \frac{k}{\epsilon} \overline{\rho u_i u_j} - \bar{u} \delta_{ij}) \frac{\partial k}{\partial x_i} \right] + \overline{\rho u_i u_j} \frac{\partial \tilde{u}_i}{\partial x_j} + \bar{\rho} \epsilon = 0 \quad (3)$$

$$L(\bar{\rho} \epsilon) = \frac{\partial}{\partial x_j} \left[\bar{\rho} \tilde{u}_j \epsilon + c_{\epsilon k} \frac{k}{\epsilon} \overline{\rho u_i u_j} \frac{\partial \epsilon}{\partial x_i} \right] + c_{\epsilon^1} \frac{\overline{u_i u_j}}{\epsilon} \frac{\partial \tilde{u}_i}{\partial x_j} + c_{\epsilon^2} \frac{\rho \epsilon^2}{k} = 0 \quad (4)$$

In equations 1-2, $\bar{\rho}$ is (constant) density, \tilde{u}_j is the mean velocity vector, \bar{p} is pressure, δ_{ij} is the Kronecker delta. The Stokes stress tensor $\bar{\sigma}_{ij}$ is defined in terms of the Reynolds number Re as

$$\bar{\sigma}_{ij} = \bar{\rho} \bar{v} (\bar{E}_{ij} - \frac{2}{3} \delta_{ij} \bar{E}_{kk}) / Re \quad (5)$$

and $\overline{\rho u_i u_j}$ is the Reynolds stress tensor. The fluid kinematic viscosity is \bar{v} , and \bar{E}_{ij} is the mean flow strain rate tensor

$$\bar{E}_{ij} \equiv \frac{\partial \bar{u}_i}{\partial x_j} + \frac{\partial \bar{u}_j}{\partial x_i} \quad (6)$$

Equations 3-4 are the transport equations for turbulent kinetic energy and isotropic dissipation function, as obtained using the closure model of Launder, Reece and Rodi [15] for the pressure-strain and triple correlations, and

$$k \equiv \frac{1}{2} \overline{u_i^2 u_i^2} \quad (7)$$

$$\epsilon \equiv \frac{2\bar{\nu}}{3} \left[\frac{\partial \bar{u}_i^2}{\partial x_j} \frac{\partial \bar{u}_j^2}{\partial x_k} \right] \delta_{jk} \quad (8)$$

The various coefficients C_β^α are model constants, Hanjalic and Launder [16].

The parabolic Navier-Stokes equation set is derived from equations 1-4 assuming the ratio of extremum transverse mean velocity component to downstream (axial) component is less than unity and that: (1.) the downstream velocity component suffers no reversal, (2.) diffusive transport processes in the downstream direction are higher-order, hence negligible, and (3.) the overall elliptic character of the parent three-dimensional Navier-Stokes equation is enforced through construction of a suitable pressure field. Viewing Figure 1 for the VSTOL jet problem, the x_1 (curvilinear) coordinate defines the predominant mean flow direction with scalar velocity component \bar{u}_1 of order unity, i.e., $O(1)$. Hence, assume $O(\bar{u}_2) \sim O(\delta) \sim O(\bar{u}_3)$ and $O(\delta) < O(1)$. Then, the continuity equation 1 confirms that the downstream variation in \bar{u}_1 must be of order equal to appropriate transverse plane variations of \bar{u}_2 and \bar{u}_3 ; hence, for $\frac{\partial}{\partial x_1} \sim O(1)$, $\frac{\partial}{\partial x_2} \approx O(\delta^{-1}) \approx \frac{\partial}{\partial x_3}$.

Determination of the relative order of terms in the Navier-Stokes equations 1-4 is straightforward, cf. reference [17]. The 3DPNS form denoted $L^P(\cdot)$, for the \bar{u}_1 momentum equation is

$$\begin{aligned} L^P(\bar{\rho}\bar{u}_1) \equiv & \frac{\partial}{\partial x_1} (\bar{\rho} \bar{u}_1 \bar{u}_1) + \frac{\partial \bar{p}}{\partial x_1} + \frac{\partial}{\partial x_2} [\bar{\rho} \bar{u}_1 \bar{u}_2 - \bar{\sigma}_{12}] \\ & + \frac{\partial}{\partial x_3} [\bar{\rho} \bar{u}_1 \bar{u}_3 - \bar{\sigma}_{13}] = 0 \end{aligned} \quad (9)$$

Should x_j correspond to a curvilinear coordinate description, the derivatives expressed in equation 9 become the covariant derivative. The order of pressure variation in the transverse plane is determined by the first order terms appearing in equation 2 written on \tilde{u}_2 and \tilde{u}_3 . Retaining the higher-order convection and laminar diffusion terms for generality, the 3DPNS form for both transverse momentum equations is [17],

$$L(\bar{p}) = \frac{\partial^2 \bar{p}}{\partial x_\ell^2} + \frac{\partial^2}{\partial x_j \partial x_\ell} \left[\bar{\rho} \tilde{u}_\ell \tilde{u}_j + \bar{\rho} \overline{u_\ell u_j} - \bar{\sigma}_{\ell j} \right] = 0 \quad (10)$$

which defines the 3DPNS limited index summation convention, $1 \leq (i, j) \leq 3$, $2 \leq \ell \leq 3$. Equation 10 is an elliptic boundary value specification for pressure distributions in the transverse plane. The pressure field that satisfies this Poisson equation is resolved into the complementary and particular solutions.

$$\bar{p}(x_i) = p_c(x_i) + p_p(x_i) \quad (11)$$

The complementary pressure is the solution to the homogeneous form of equation 10. The particular pressure p_p satisfies equation 10, subject to homogeneous Dirichlet boundary conditions on boundary segments where p_c is known. The 3DPNS form for equations 3-4 is

$$\begin{aligned} L^P(k) = & \frac{\partial}{\partial x_i} (\bar{\rho} \tilde{u}_i k) + \frac{\partial}{\partial x_i} \left[\bar{\rho} (C_k \frac{k}{\epsilon} \overline{u_i u_\ell} - \bar{\nu} \delta_{i\ell}) \frac{\partial k}{\partial x_\ell} \right] \\ & + \bar{\rho} \overline{u_i u_\ell} \frac{\partial \tilde{u}_1}{\partial x_\ell} + \bar{\rho} \epsilon = 0 \end{aligned} \quad (12)$$

$$\begin{aligned} L^P(\epsilon) = & \frac{\partial}{\partial x_i} (\bar{\rho} \tilde{u}_i \epsilon) + \frac{\partial}{\partial x_i} \left[C_\epsilon \frac{k}{\epsilon} \overline{u_i u_\ell} \frac{\partial \epsilon}{\partial x_\ell} \right] \\ & + C_\epsilon^1 \bar{\rho} \overline{u_i u_\ell} \frac{\epsilon}{k} \frac{\partial \tilde{u}_1}{\partial x_\ell} + C_\epsilon^2 \bar{\rho} \frac{\epsilon^2}{k} = 0 \end{aligned} \quad (13)$$

With determination of equation 10 as governing first-order phenomena, it is necessary to retain the $O(\delta)$ transverse momentum equations to permit determination of \bar{u}_ℓ . Retaining the highest two orders of terms, the corresponding $O(\delta)$ transverse momentum equations are

$$L^\delta(\bar{\rho}\bar{u}_k) = \frac{\partial}{\partial x_1} \left[\bar{\rho}\bar{u}_1\bar{u}_k + \overline{\rho u_1 u_k} \right] + \frac{\partial}{\partial x_\ell} \left[\bar{\rho}\bar{u}_\ell\bar{u}_k + \overline{\rho u_\ell u_k} + \bar{p}\delta_{k\ell} - \bar{\sigma}_{k\ell} \right] = 0 \quad (14)$$

Equation 12 employs the additional limited index $2 \leq k \leq 3$. The middle two terms in the second bracket are $O(1)$, while the remaining terms are all $O(\delta)$. As a consequence of using equation 14, it becomes necessary to enforce the first-order effects of the continuity equation 1 directly on its solution. The theoretical concept is to enforce a measure of the continuity equation (solution) as a differential constraint on solution of the $O(\delta)$ transverse momentum equations 14. This solution measure is chosen as the harmonic function $\phi(x_\ell)$, the solution to the Poisson equation

$$L^P(\phi) \equiv \frac{\partial^2 \phi}{\partial x_\ell^2} - \frac{\partial}{\partial x_1} (\bar{\rho} \bar{u}_1) \equiv 0 \quad (15)$$

The boundary conditions for ϕ are homogeneous Dirichlet everywhere at farfield.

Reynolds Stress Closure Model for 3DPNS

A closure model for the kinematic Reynolds stress $-\overline{u_i u_j}$, appearing in equations 9-13 is required. A stress-strain rate constitutive equation yields the kinematic form [17],

$$-\overline{u_i u_j} = -\alpha_{ij} + C_4 \frac{k^2}{\epsilon} \bar{E}_{ij} + C_2 C_4 \frac{k^3}{\epsilon^2} \bar{E}_{ik} \bar{E}_{kj} + \dots \quad (16)$$

where \bar{E}_{ij} is the symmetric mean flow strain-rate tensor given in equation 6. Retaining terms of the first two orders of significance, the 3DPNS form for the Reynolds stress tensor is

$$\begin{array}{ll}
\begin{array}{l}
\overline{-u_1^2 u_1^2} = C_1 k - C_2 C_4 \frac{k^3}{\epsilon^2} \left[\left(\frac{\partial \bar{u}_1}{\partial x_2} \right)^2 + \left(\frac{\partial \bar{u}_1}{\partial x_3} \right)^2 \right] \\
\overline{-u_2^2 u_2^2} = C_3 k - C_2 C_4 \frac{k^3}{\epsilon^2} \left[\frac{\partial \bar{u}_1}{\partial x_2} \right]^2 \\
\overline{-u_3^2 u_3^2} = C_3 k - C_2 C_4 \frac{k^3}{\epsilon^2} \left[\frac{\partial \bar{u}_1}{\partial x_3} \right]^2 \\
\overline{-u_1^2 u_2^2} = - C_4 \frac{k^2}{\epsilon} \left[\frac{\partial \bar{u}_1}{\partial x_2} \right] \\
\overline{-u_1^2 u_3^2} = - C_4 \frac{k^2}{\epsilon} \left[\frac{\partial \bar{u}_1}{\partial x_3} \right] \\
\overline{-u_2^2 u_3^2} = - C_2 C_4 \frac{k^3}{\epsilon^2} \left[\frac{\partial \bar{u}_1}{\partial x_2} \frac{\partial \bar{u}_1}{\partial x_3} \right]
\end{array}
&
\begin{array}{l}
O(\delta^2) \\
- 2 C_4 \frac{k^2}{\epsilon} \left[\frac{\partial \bar{u}_2}{\partial x_1} \right] \\
- 2 C_4 \frac{k^2}{\epsilon} \left[\frac{\partial \bar{u}_2}{\partial x_2} \right] \\
- 2 C_4 \frac{k^2}{\epsilon} \left[\frac{\partial \bar{u}_2}{\partial x_3} \right] \\
- C_2 C_4 \frac{k^3}{\epsilon^2} \left[\frac{\partial \bar{u}_1}{\partial x_3} \left(\frac{\partial \bar{u}_2}{\partial x_3} + \frac{\partial \bar{u}_3}{\partial x_2} \right) \right. \\
\quad \left. + 2 \frac{\partial \bar{u}_1}{\partial x_2} \left(\frac{\partial \bar{u}_1}{\partial x_1} + \frac{\partial \bar{u}_2}{\partial x_2} \right) \right] \\
- C_2 C_4 \frac{k^3}{\epsilon^2} \left[\frac{\partial \bar{u}_1}{\partial x_2} \left(\frac{\partial \bar{u}_2}{\partial x_3} + \frac{\partial \bar{u}_3}{\partial x_2} \right) \right. \\
\quad \left. + 2 \frac{\partial \bar{u}_1}{\partial x_3} \left(\frac{\partial \bar{u}_1}{\partial x_1} + \frac{\partial \bar{u}_2}{\partial x_2} \right) \right] \\
- C_4 \frac{k^2}{\epsilon} \left[\frac{\partial \bar{u}_2}{\partial x_3} + \frac{\partial \bar{u}_3}{\partial x_2} \right]
\end{array}
\end{array}
\quad (17)$$

Finite Element Solution Algorithm

The 3DPNS equation system has been identified for the dependent variable set $q_j(x_i) \equiv \{q\} = \{\bar{u}_1, \bar{u}_2, \bar{u}_3, \bar{p}, k, \epsilon\}^T$. The governing system includes equations 1, 9, 10, 12, 13 and 15. Equations 9, 12 and 13 contain the initial value term that permits a space-marching procedure. Equation 10 is an elliptic boundary value problem with parametric initial-value dependence. The continuity equation 1 solution becomes recast and utilized as a differential constraint.

The generalized form for the 3DPNS equation set is,

$$L^P(q_j) = \frac{\partial}{\partial x_1} (\bar{\rho} \bar{u}_1 q_j) + \frac{\partial}{\partial x_2} [\rho \bar{u}_2 q_j + f_{2j}] + s_j = 0 \quad (18)$$

where f_{2j} and s_j are specified nonlinear functions of their arguments as determined by the index j . The solution domain Ω is defined as the region $Z > 0$ in Figure 1.

The finite element numerical solution algorithm for equation 16 defines the approximation $q_j^h(x_\ell, x_1)$, to the (unknown) exact solution $q_j(x_\ell, x_1)$, as

$$q_j(x_\ell, x_1) \approx q_j^h(x_\ell, x_1) \equiv \bigcup_{e=1}^M q_j^e(x_\ell, x_1) \quad (19)$$

Planes $Z = C$ are discretized into a finite element distribution and in each finite element R_e^2 , the elemental approximation is

$$q_j^e(x_\ell, x_1) \equiv \{N_k(x_\ell)\}^T \{QJ(x_1)\}_e \quad (20)$$

In equations 19-20, $j(J)$ is a free index denoting members of $\{q^h\}$, and sub- or superscript e denotes pertaining to the e^{th} finite element, $\Omega_e \equiv R_e^2 \times x_1$. The elements of the row matrix $\{N_k(x_\ell)\}^T$ are linear ($k = 1$) polynomials on x_ℓ , $2 \leq \ell \leq 3$, spanning triangles.

The finite element algorithm requires the generated error $L^P(q_j^h)$ to be orthogonal to the functions $\{N_k\}$ employed to define q_j^h . In addition, the discrete approximation $L^P(\bar{\rho}^h)$ to the continuity equation is enforced as a differential constraint on $L^\delta(\bar{\rho} \bar{u}_\ell^h)$. The theoretical statement of the finite element solution algorithm is then

$$\int_{R^2} \{N_k\} L^P(q_j^h) d\vec{x} + \beta_1 \int_{R^2} \nabla \{N_k\} L^P(\bar{\rho}^h) d\vec{x} \equiv \{0\} \quad (21)$$

Equation 21 defines a system of ordinary differential equations written in the jet direction parallel to x_1 in the form

$$[C]\{QJ\}' + [U]\{QJ\} + [FLJ]\{QL\} + \{SJ\} = \{0\} \quad (22)$$

Using the trapezoidal integration rule,

$$\{FJ\} \equiv \{QJ\}_{j+1} - \{QJ\}_j - \frac{\Delta x_1}{2} [\{QJ\}'_{j+1} + \{QJ\}'_j] \equiv \{0\} \quad (23)$$

and substituting equation 22 defines a system of nonlinear algebraic equations for determination of the elements of $\{QJ(x_1)\}$. The Newton iteration algorithm for equation 23 is

$$[J(FJ)]_{j+1}^p \{\delta QJ\}_{j+1}^{p+1} = - \{FJ\}_{j+1}^p \quad (24)$$

and

$$\{QJ\}_{j+1}^{p+1} \equiv \{QJ\}_{j+1}^p + \{\delta QJ\}_{j+1}^{p+1} \quad (25)$$

Additional details on the algorithm are given in reference [17]. The algorithm is operational in the COMOC:3DPNS computer program [18].

DISCUSSION AND RESULTS

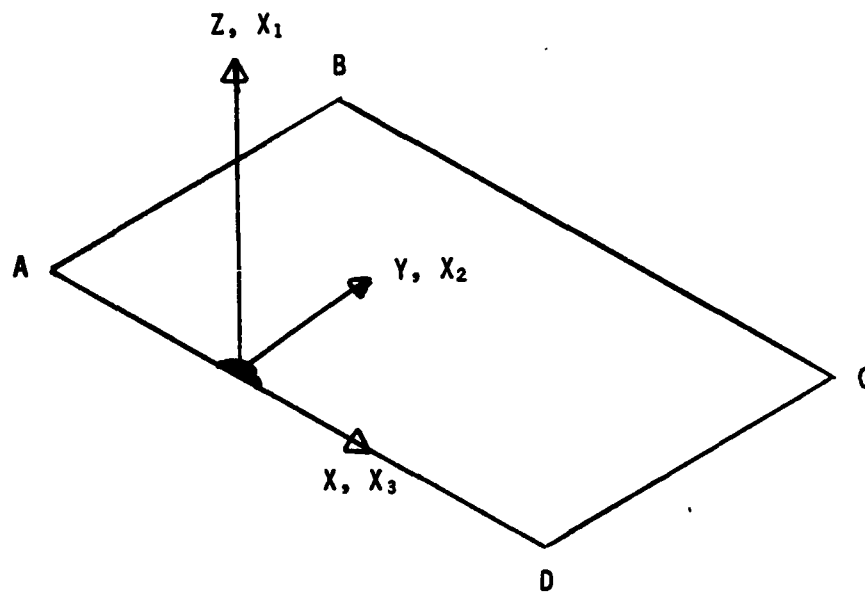
Problem Specification

The analysis of a VSTOL jet in cross-flow, using the 3DPNS computational simulation, requires specification of the following:

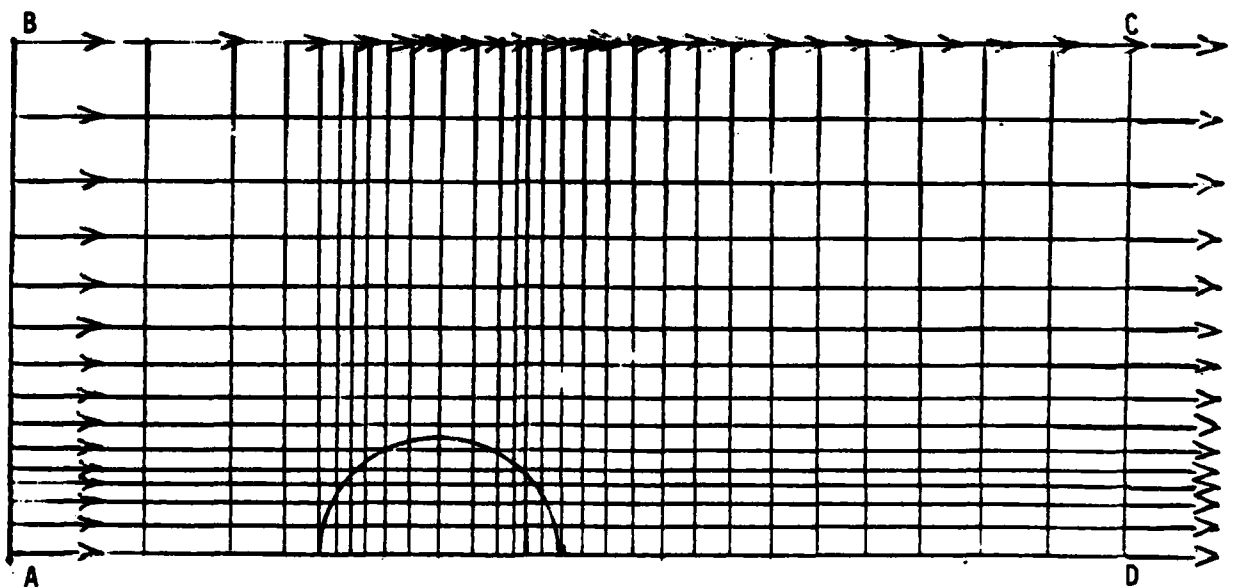
- a) Solution domain extent, $\Omega = R^2 \times x_1$
- b) Boundary conditions for $q_i^h(x_i)$ on $\partial\Omega = \partial R \times x_1$
- c) Initial conditions for $q_i^h(x_i)$ on $\Omega_0 = R^2 \times x_1(0)$
- d) Estimation of the x_1 pressure gradient for the \tilde{u}_1 momentum equation.

Recalling Figure 1, the solution domain is the region $Z > 0$, and of sufficient lateral extent to permit specification of boundary conditions corresponding to the imposition of cross-flow. Since the plane $Y = 0$ is a plane of symmetry, only one-half of the physical problem need be discretized. Figure 8a) is a sketch of the 3DPNS domain Ω , denoted by vertex array A-B-C-D and including the region $Z > 0$. Since for $\lambda = 8$, the jet axis does not exhibit significant curvature on $0 \leq Z/D < 5$, Figure 5, the 3DPNS coordinate system x_i is coincident with the laboratory reference frame X, Y, Z . The 3DPNS solution is marched parallel to the x_1 (Z) axis.

Since the 3DPNS equation system is an elliptic boundary value description in the x_2 - x_3 plane, A-B-C-D in Figure 8a), a boundary condition statement is required for every member of $q_i^h(x_1, x_2)$. On D-A, the symmetry plane, each dependent variable is assumed to exhibit a vanishing normal derivative, i.e., $\partial q_i^h / \partial x_2 = 0$ on D-A. Boundary segment A-B corresponds to the upstream cross-flow boundary, whereupon $\tilde{u}_2 = U_\infty(-\hat{j})$, and k and ϵ are specified as a function of location within the boundary layer assumed attached to the x_2 - x_3 plane. Both \tilde{u}_1 and \tilde{u}_3 are assumed to exhibit vanishing normal derivatives on A-B. Boundary segment B-C is assumed sufficiently remote from the jet that the onset flow $U_\infty(-\hat{j})$ proceeds unaltered parallel to B-C. All other dependent variables are assumed to exhibit vanishing normal derivatives, specifically including \tilde{u}_3 , the computed non-zero level of which will correspond to deflection and/or entrainment of the cross-flow by the jet interaction. Boundary segment D-C is assumed located sufficiently downstream from the jet such that the imposed cross-flow is recovered, i.e., $\tilde{u}_2(x_1, x_2 = B-C) = U_\infty(-\hat{j})$.



a) 3DPNS Solution Domain Ω .



b) Transverse Solution Domain Discretization UR_e^2 .

Figure 8. 3DPNS Computational Simulation Solution Domain.

All other variables are assumed to exhibit vanishing normal derivatives on segment C-D. Figure 8b) is a graph of the discretization $R^2 = UR_e^2$, with the cross-flow distribution imposed on the boundary.

The initial condition specification for $q_i^h(x_1(0), x_2)$ on $\Omega_0 = R^2 \times x_1(0)$ defines the basic problem and consists principally of the jet cross-flow velocity ratio and the character of the boundary layer region adjacent to the plane of injection. As discussed at length in reference [17], it is necessary to augment the velocity component parallel to x_1 by a small constant background level to render the 3DPNS description nonsingular. For a velocity ratio of $\lambda \equiv U_j/U_\infty = 8$, the background level for $\tilde{u}_1(x_1, x_2) = 0.2 U_j$ was determined acceptable and used for these studies. The jet is defined to exist in a semi-circular region of Ω_0 centered on the x_1 axis, Figure 8. The imposed cross-flow \tilde{u}_2 is assumed to exist only on the boundary segments A-B-C of $\partial\Omega$, starting at a zero level at $x_1 = 0$ and proceeding through a boundary-layer type evolution until $\tilde{u}_2 = U_\infty(-\hat{j})$ at some specified distance above the injection plane, say $x_1/D \sim 1.0$. The initial condition for \tilde{u}_2 everywhere interior to $\partial\Omega$, and for \tilde{u}_3 except on segment A-B, is self-generated by the 3DPNS analysis by the action of the continuity constraint numerical algorithm. The initial distributions for k and ϵ proceed through a similar boundary layer development.

Algorithm Specification

Recalling the ordering analysis yielding the 3DPNS simplification, the transverse plane momentum equations were determined to govern pressure distributions via a Poisson equation. The VSTOL problem specification presents a significant challenge in that the complementary pressure solution is a uniform constant since the inviscid flowfield exterior to the domain Ω is uniform. The particular pressure solution contains the entire pressure distribution resulting from the action of generated Reynolds stress and transverse plane velocity field distributions. However, no initial specification can be completed since there is no knowledge of the Reynolds stress and velocity field distributions on the interior of Ω and near the injection plane $Z \sim 0$. This is not a critical issue with the transverse plane velocity solution \tilde{u}_2 since first-order effects are governed by the continuity equation.

However, the first-order momentum equation for \tilde{u}_1 contains the x_1 -pressure gradient as a source term, and an estimate is required to achieve the first solution.

The resolution of this issue was accomplished in this study by definition of a "virtual region" with an auxiliary pressure gradient computation, and an interaction procedure involving multiple overlapping 3DPNS solutions. The "virtual region" computation is the first 3DPNS solution generated on the span $0 \leq x_1/D < 1.0$, i.e., marching from the injection plane a distance of up to one jet diameter parallel to the jet. In this region it is assumed that the momentum imparted to the jet flow by the injection process is maintained nominally constant in an overall integrated sense. The measure of the x_1 momentum is the integral

$$\bar{m}_1 \equiv \int_{R^2} \bar{\rho} \tilde{u}_1^h d\vec{x} = \sum_{e=1}^m \int_{R_e^2} \bar{\rho} \tilde{u}_1^e d\vec{x} \quad (26)$$

The last form of equation 26 is the sum of integrals over the two dimensional plane of the discretization, Figure 8b). An axial (x_1) pressure gradient is computed, from the change in momentum computed from equation 26, according to the definition

$$\frac{d\bar{p}}{dx_1} \equiv \frac{-\Delta(\bar{m}_1)}{A_j} = \frac{-(\bar{m}_1(x_1) - \bar{m}_0)}{A_j} \quad (27)$$

In equation 27, A_j is the cross-sectional area occupied by the jet at the injection plane, i.e., the area of the finite element domains interior to the semi-circle defining the jet, Figure 8b).

The solution of equation 27 is a scalar estimate of the pressure gradient parallel to the x_1 axis required to maintain the mean momentum of the jet. The remainder of the 3DPNS algorithm is solved, as discussed in the previous section, specifically including the particular pressure field which is written onto an output file at preselected stations on $0 < x_1/D < 0.5$. In addition, the entire virtual region 3DPNS solution dependent variable set is written

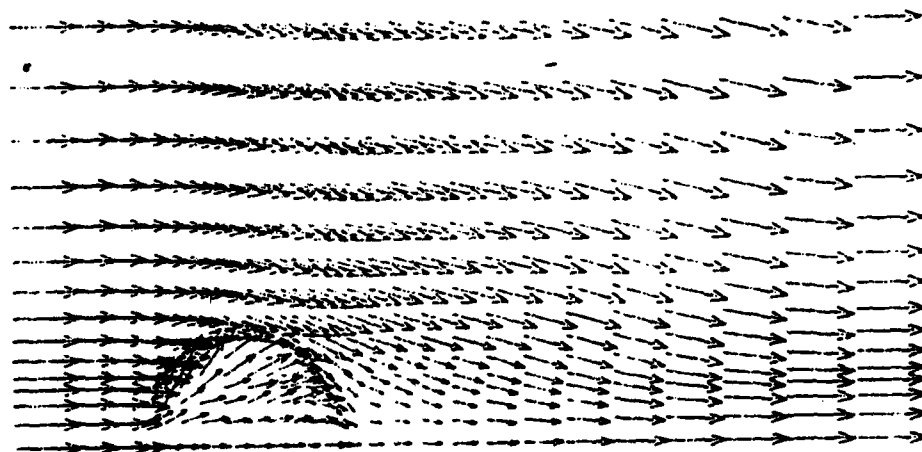
onto the output file at a pre-determined axial station, say $X_1/D = 0.25$, to serve as a new set of initial conditions for the subsequent interaction solution.

The first interaction solution overlaps the virtual region solution on $0.25 \leq X_1/D \leq 0.5$, and extends further downstream parallel to the jet axis to $X_1/D = 1.0$. On the overlap region, the axial pressure gradient for the \bar{u}_1 momentum equation is constructed by differencing the stored particular pressure distributions from the virtual region solution. The last pressure gradient, computed in this manner, is also extrapolated and used for the 3DPNS solution on the extended region $0.5 \leq X_1/D \leq 1.0$. The first interaction solution particular pressure distributions are utilized directly in the transverse momentum equation solutions, as well as written onto the output file at preselected axial stations for use in the second interaction solution.

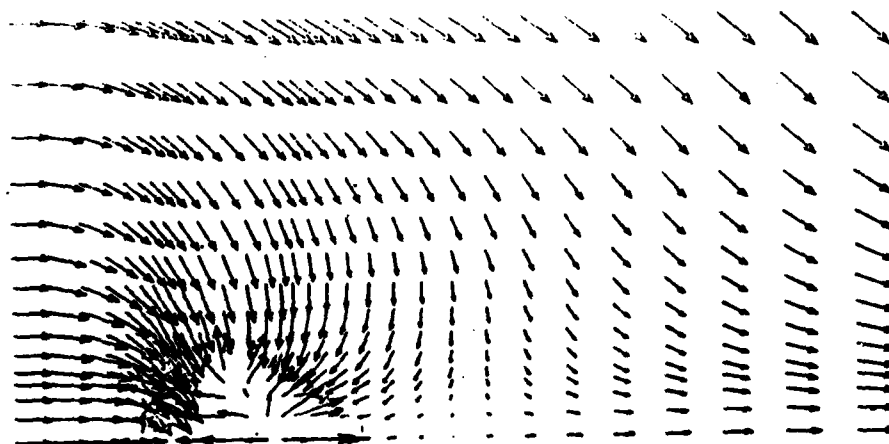
The second, and subsequent interaction solutions are restarted at $X_1/D = 0.25$, or further along the jet axis, using the most recent 3DPNS solution particular pressure distributions to compute the pressure gradient for the \bar{u}_1 momentum equation. Each subsequent interaction solution is carried progressively further downstream along the jet axis than the span for which the pressure distributions have been computed from the previous solution. Within each solution, however, the current particular pressure solution is employed in a non-delayed manner in the transverse plane momentum equations. In this manner, item d) of the 3DPNS analysis requirements is met, assuming that the pressure gradient iteration procedure is convergent and yields flowfield predictions in agreement with experimental data.

Circular Jet Analysis

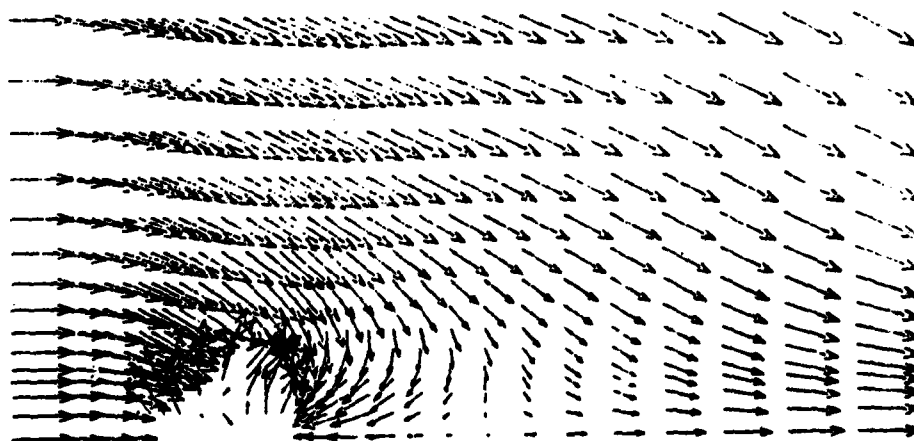
The principal requirement is to verify the developed 3DPNS procedure for prediction of the near-field flowfield evolution of a circular cross-section VSTOL jet at $\lambda = 8$. Figure 9 summarizes the virtual region solutions in terms of computed velocity vector distributions in the half-plane transverse to the jet axis at $X_1/D = 0.25$. Without the imposition of a pressure gradient in the \bar{u}_1 momentum equation, the applied crossflow immediately penetrates into the jet region, Figure 9a). Even though the periphery of the jet is well defined, this penetration is at variance with the experimental data, Figure 7a).



a) $d\bar{p}/dx = 0$, Equation 27



b) $d\bar{p}/dx \neq 0$, Equation 27



c) $d\bar{p}/dx = 0$ and $\bar{u}_2(c) = 0$

Figure 9. Comparison of 3DPNS Virtual Region Solution, Transverse Velocity Distributions, Circular Cross-Section VSTOL Jet, $\lambda = 8.$, $X_1/D = 0.25$.

Computing the X_1 direction pressure gradient, according to equation 27, and applying it yields the \tilde{u}_ℓ velocity distribution shown in Figure 9b). There occurs a pronounced turning of the crossflow towards the jet, and a stagnation point is predicted about one-half diameter downstream of the jet boundary in the wake region. However, substantial \tilde{u}_2 velocities are still predicted on the jet centerline. For comparison, deleting the pressure gradient computation and defining $\tilde{u}_2 \equiv 0$ on the centerline within the jet, yields the prediction shown in Figure 9c), which differs in only a small way from Figure 9b).

These results indicate that the virtual region computation, with momentum conserving pressure gradient, can produce an initialization for the subsequent 3DPNS solutions that is acceptable. The pressure gradient application is crucial in that without it the crossflow always penetrates the jet. A sequence of additional computations confirm that the principal action of the pressure gradient is to counter-balance the strong turbulent mixing on the upstream face of the jet. Without this balance, a large x_1 -derivative of \tilde{u}_1 results, ie., $\partial \tilde{u}_1 / \partial x_1 \ll 0$. Since $\tilde{u}_3 = 0$ and $\partial \tilde{u}_3 / \partial x_3 \approx 0$ on the symmetry centerplane and within the jet, the balancing of first order effects controlled by the continuity equation must yield generation of a significant velocity component \tilde{u}_2 . The momentum conserving pressure gradient computation serves to balance this coupling mechanism within the continuity equation.

Figure 10 summarizes the 3DPNS virtual region \tilde{u}_ℓ solution on $0.5 \leq X_1/D \leq 1.0$, as generated using the momentum conserving pressure gradient. For this solution, the \tilde{u}_2 velocity component on the symmetry plane within the jet was also set to zero. At $X_1/D = 0.5$, there appears a nominal radial outflow within the jet region, a wake stagnation point about $0.5D$ downstream, and a beginning indication of entrainment from the wake, Figure 10a). There is little qualitative change in the appearance of this transverse plane velocity distribution on $0.5 < X_1/D \leq 1.0$, except for elimination of the rear wake stagnation point.

The principal requirement of the solution of Figure 10 is to provide a particular pressure distribution for the \tilde{u}_1 momentum equation for the first interaction solution. Since the data of Figure 10 exhibit some level of qualitative agreement with the experimental data of Fearn et al, Figure 7, the first interaction can be executed. For this and subsequent solutions,

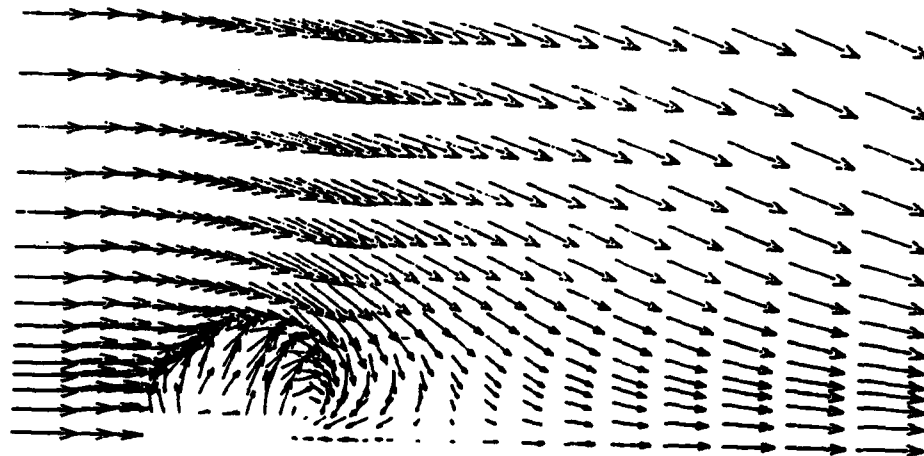
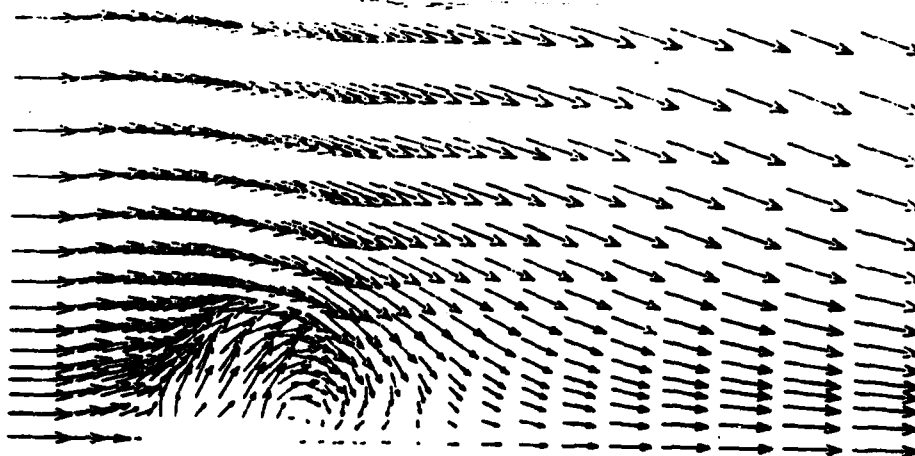
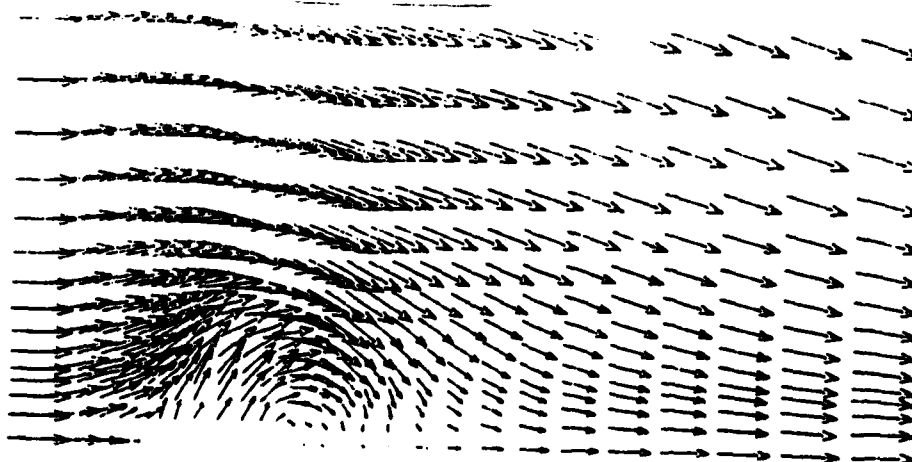
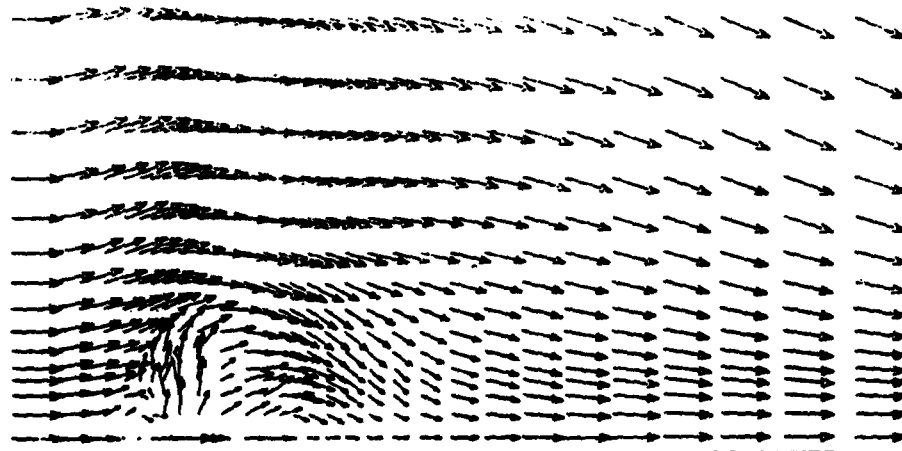
a) $X_1/D = 0.5$ b) $X_1/D = 0.75$ c) $X_1/D = 1.0$

Figure 10. Summary of 3DPNS Virtual Region Solution, Transverse Velocity Distributions, $\bar{u}_2 \equiv 0$ on Symmetry Plane, Circular Cross-Section VSTOL Jet, $\lambda = 8$.

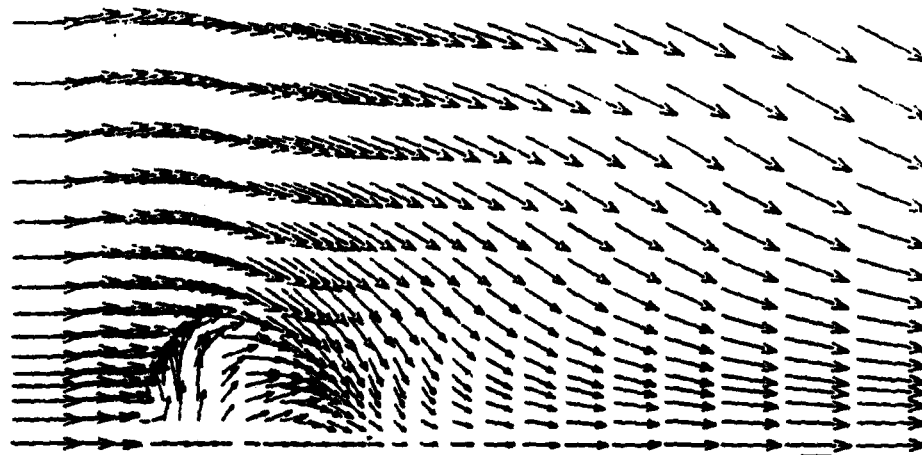
\bar{u}_2 on the symmetry plane within the jet is released and computed assuming a vanishing normal derivative boundary condition. Figure 11 summarizes the first solution as transverse plane velocity distributions. The boundary of the jet is clearly defined at $X_1/D = 0.5$, and the jet deflection action on the crossflow is quite evident. Particularly encouraging is the almost purely transverse outflow velocity \bar{u}_3 , computed in the forward half of the jet region on $0.5 \leq X_1/D \leq 1.0$. This action is in quite good qualitative agreement with the data, Figure 7a). Also, this solution gives almost no evidence of a roll-up of a secondary vortex is indicated by the data. However, intrusion of a relatively large component of \bar{u}_2 occurs, interior to the jet at $X_1/D = 1.0$, which does not agree with the indications of the experimental data.

Figure 12 summarizes the second interaction solution on $0.75 \leq X_1/D \leq 1.25$. A rather substantial increase in entrainment action is indicated at $X_1/D = 0.75$, in comparison to Figure 11b), and a nominal transverse outflow for \bar{u}_3 is maintained on the jet interior. Further, a wake region stagnation point has reappeared which persists to $X_1/D = 1.25$. However, the \bar{u}_2 mass flux through the jet core region persists at $X_1/D = 1.0$, and is even more pronounced at $X_1/D = 1.25$.

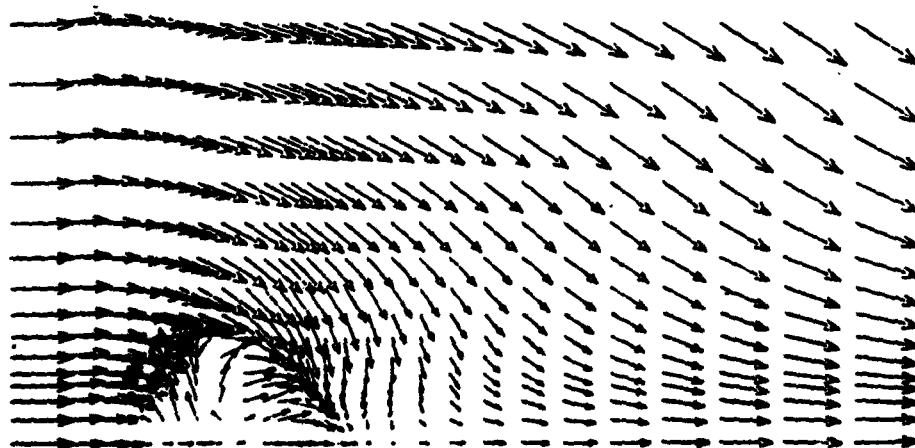
These 3DPNS predictions indicate that the lack of knowledge regarding the detailed distribution of axial pressure gradient in the \bar{u}_1 momentum equation is a constraint. Even with this limitation, however, a substantial quantitative assessment of a plausible nearfield evolution of the crossflow has been generated. In particular, Figure 13 is a graph of pressure coefficient distribution $C_p = 1 - \bar{\rho} \bar{u}_\infty^2 / \rho_\infty U_\infty^2$ on the plane $X_3/D = 0.75$. Assuming that exterior to the jet region this pressure distribution is nominally imposed through the crossflow boundary layer, the general distribution of isobars is in qualitative agreement with data [10]. In particular, the extremum level on the lateral downstream side of the jet is due directly to the strong entrainment velocity field predicted by the 3DPNS solution and confirmed by many experiments. Further, Figure 13b) is a plot of isovels of the jet direction velocity distribution \bar{u}_1 . The initially semi-circular contours have been noticeably bowed laterally in the direction perpendicular to the imposed crossflow. This is also in good qualitative agreement with data, cf. Figure 4a), and is solely the result of



a) $X_1/D = 0.5$



b) $X_1/D = 0.75$



c) $X_1/D = 1.0$

Figure 11. Summary of First Interaction Solution Transverse Plane
Velocity Distributions, Circular Cross-Section VSTOL Jet, $\lambda = 8$.

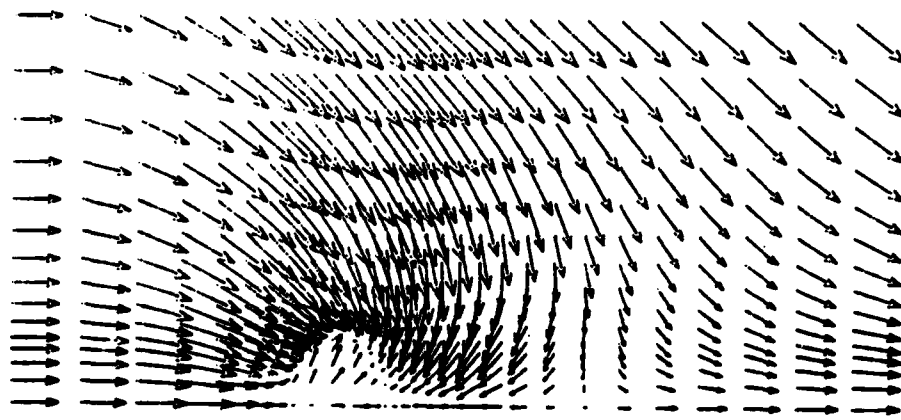
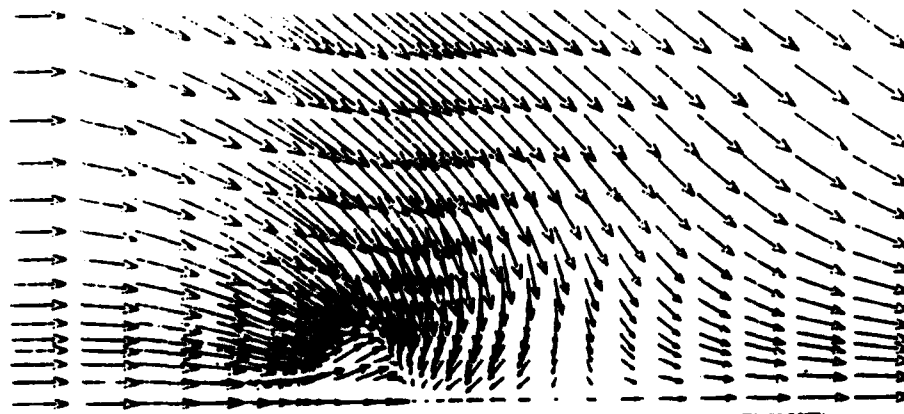
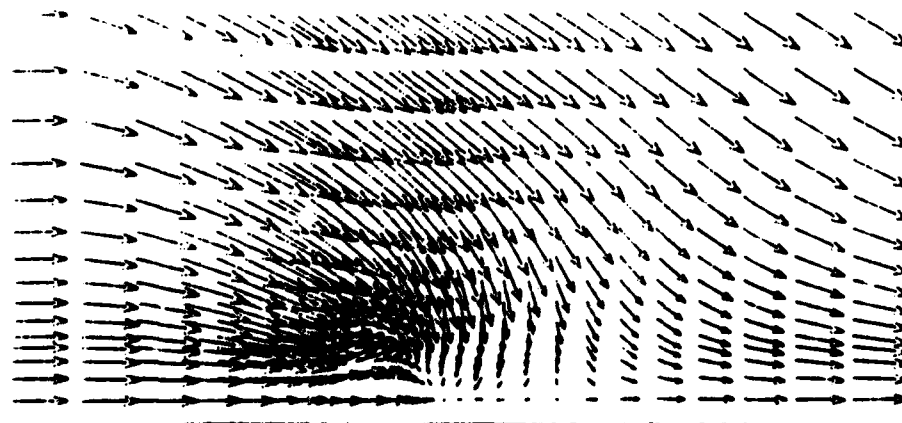
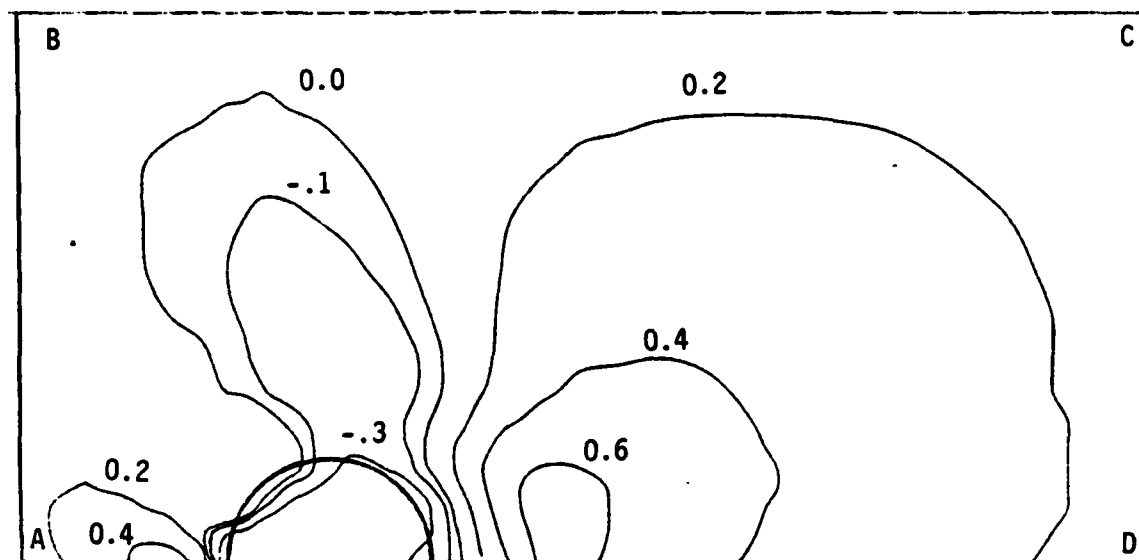
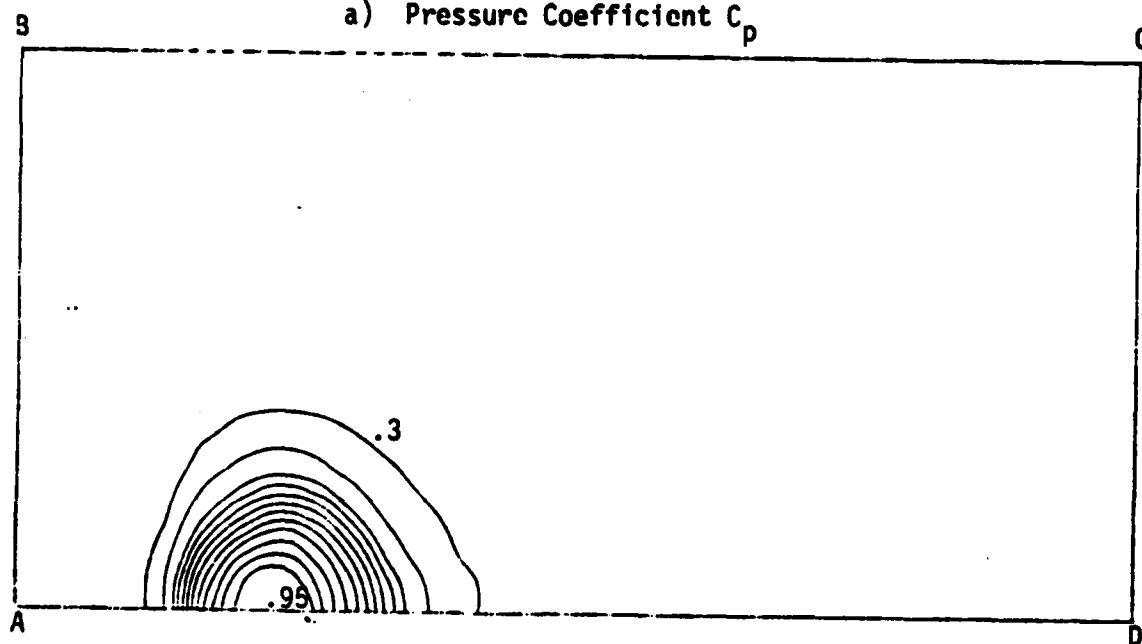
a) $X/D_1 = 0.75$ b) $X_1/D = 1.0$ c) $X_1/D = 1.25$

Figure 12. Summary of Second Interaction Solution Transverse Plane Distributions, Circular Cross Section VSTOL Jet, $\lambda = 8.0$



a) Pressure Coefficient C_p



b) Axial Velocity \bar{u}_1 .

Figure 13. Second Interaction Solution Fields, Circular Cross-Section
VSTOL Jet, $\lambda = 8$, $x_1/D = 0.75$.

the induced transverse plane velocity field \tilde{u}_ℓ .

As discussed, the pressure field computed in the 3DPNS algorithm responds to first-order to the Reynolds stress distributions, coupled to lower order with the transverse velocity field, see equation 11. The accuracy of the 3DPNS solution depends critically therefore on the stress distributions. Figure 14 summarizes the second interaction solution prediction of the Reynolds normal stress distributions at $X_1/D = 0.75$. All three components exhibit profile contours geometrically similar to the \tilde{u}_1 isovel distribution, with the peak levels coincident with the extremum gradients in \tilde{u}_1 . Figure 15 graphs the corresponding 3DPNS solution for Reynolds shear stress distributions at $X_1/D = 0.75$. The extremum gradients in $\overline{u_1 u_2}$ and $\overline{u_1 u_3}$ are parallel to the corresponding transverse coordinate direction \tilde{u}_ℓ , as expected. It would be highly informative to have experimental data for comparison of these predictions.

SUMMARY AND CONCLUSIONS

A three-dimensional parabolic Navier-Stokes numerical solution algorithm has been analyzed for prediction of the nearfield flow development of a VSTOL jet in subsonic crossflow. The essential aspects of algorithm definition, with regards to initial and boundary condition specifications, has been summarized. A momentum conserving pressure gradient computation has been developed to complete the problem definition and facilitate problem initialization. A sequence of overlapping interaction solutions has been evaluated for prediction of a circular jet at $\lambda = 8.0$. The results of the 3DPNS predictions have compared qualitatively with the sparse available experimental data. It is crucial that quality data be acquired to permit quantitative assessment of the results of this analysis procedure.



a) Axial Normal Stress $\overline{u_1 u_1}$

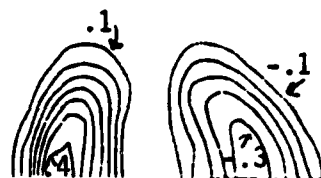


b) Transverse Normal Stress $\overline{u_2 u_2}$

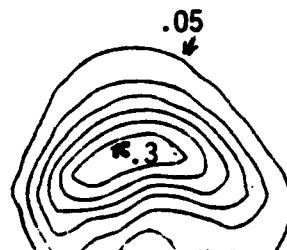


c) Transverse Normal Stress $\overline{u_3 u_3}$

Figure 14. Second Interaction Solution Reynolds Normal Stress Distributions, Circular Cross-Section VSTOL Jet, $\lambda = 8$, $X/D = 0.75$.



a) Reynolds Shear Stress $\overline{u_1 u_2}$



b) Reynolds Shear Stress $\overline{u_1 u_3}$



c) Reynolds Shear Stress $\overline{u_2 u_3}$

Figure 15. Second Interaction Solution Reynolds Shear Stress Distributions. Circular Cross-Section VSTOL Jet, $\lambda = 8$, $X_1/D = 0.75$.

REFERENCES

1. Chang, H. C., "The Roll-Up Of A Cylindrical Jet In A Cross-Flow," Aerospace Research Laboratories Report ARL 73-0131, 1973.
2. Wooler, P. T., "Development Of An Analytical Model For The Flow Of A Jet Into A Subsonic Cross-Wind," NASA SP-218, p. 101-118, 1968.
3. Schmidt, H., "Deflection Of A Round Turbulent Jet In A Cross-Wind," Arch. Mech., Vol. 26, Pt. 5, p. 849-859, 1974.
4. Jordinson, R., "Flow In A Jet Directed Normal To The Wind," ARC Report And Memoranda No. 3074, 1956.
5. Moussa, A. F., Trischka, J. W. and Eskinazi, F., "The Near Field In The Mixing Of A Round Jet With A Cross-Stream," J. Flu. Mech., Vol. 80, Pt. 1, p. 49-80, 1977.
6. Vogler, R. D., "Surface Pressure Distributions Induced On A Flat Plate By A Cold Air Jet Issuing Perpendicularly From The Plate And Normal To A Low-Speed Free Stream Flow," NASA TN D-1629, 1963.
7. Bradbury, L. J. S., and Wood, M. N., "The Static Pressure Distribution Around A Circular Jet Exhausting Normally From A Plane Wall Into An Airstream," C. P. No. 822, 1965, British Aero. Res. Council.
8. McMahon, H. M. and Mosher, D. K., "Experimental Investigation Of Pressures Induced On A Flat Plate By A Jet Issuing Into A Subsonic Crosswind," NASA SP-218, p. 49-62, 1968.
9. Margason, R. J. and Fearn, R., "Jet-Wake Characteristics And Their Induced Aerodynamic Effects On V/STOL Aircraft In Transition Flight," NASA SP-218, p. 1-18, 1968.
10. Kamotani, Y. and Greber, I., "Experiments On A Turbulent Jet In A Cross-Flow," AIAA J., Vol. 10, No. 11, p. 1425-29, 1972.
11. Fearn, R. and Weston, R. P., "Vorticity Associated With A Jet In A Cross-Flow," AIAA J., Vol. 12, No. 12, p. 1666-1671, 1974.
12. Fearn, R. L. and Benson, J. P., "Velocity Field Near The Jet Orifice Of A Round Jet In A Crossflow," Technical Report NASA-CR-152293, 1981.
13. Baker, A. J., Orzechowski, J. A. and Manhardt, P. D., "A Numerical Three-Dimensional Turbulent Simulation Of A Subsonic Interaction VSTOL Jet In Crossflow Using A Finite Element Algorithm," Technical Report NADC-79021-60, 1981.
14. Cebeci, T. and Smith, A. M. O. Analysis Of Turbulent Boundary Layers, Academic Press, New York, 1974.

15. Launder, B. E., Reece, G. J. and Rodi, W., "Progress in the Development of a Reynolds-Stress Turbulence Closure," J. Flu. Mech., V. 68, Pt. 3, pp. 537-566, 1975.
16. Hanjalic, K. and Launder, B. E., "A Reynolds Stress Model of Turbulence and its Application to Thin Shear Flows," J. Flu. Mech., V. 52, Pt. 4, pp. 609-638, 1972.
17. Baker, A. J. and Orzechowski, J. A., "A Continuity Constraint Finite Element Algorithm for Three-Dimensional Parabolic Flow Prediction," Technical Paper Presented At ASME Winter Annual Meeting, Washington, DC, Nov. 1981.
18. Manhardt, P. D., "C M C:3DPNS Computer Program User's Manual," Final Report For NASA Contract NAS1-15105, 1982.

DISTRIBUTION LIST

REPORT NO. NADC-81177-60
CONTRACT NO. N62269-81C-0395

| | No. of Copies |
|--|---------------|
| Naval Air System Command | 7 |
| (2 for AIR-00D4) | |
| (2 for AIR-3110) | |
| (1 for AIR-5301) | |
| (1 for AIR-31) | |
| (1 for PMA-257) | |
| Naval Weapons Center | 1 |
| (1 for Commander) | |
| Naval Air Propulsion Center | 1 |
| (1 for Commanding Officer) | |
| Naval Air Test Center | 1 |
| (1 for Commander) | |
| David W. Taylor Naval Ship Research and Development Center | 1 |
| (1 for Commander) | |
| Office of Naval Research | 2 |
| (1 for Chief) | |
| (1 for Dr. R. Whitehead) | |
| Institute of Defense Analysis | 1 |
| (1 for J. Attinello) | |
| Naval Postgraduate School | 1 |
| (1 for Superintendent) | |
| NASA, Ames Research Center | 1 |
| (1 for S. Anderson) | |
| NASA, Edwards AFB | 1 |
| (1 for Director) | |
| NASA, Langley Research Center | 1 |
| (1 for Director) | |
| NASA, Lewis Research Center | 1 |
| (1 for Director) | |
| USAF Flight Dynamics Laboratory | 1 |
| (1 for ASD/ENFDH) | |
| USAF Aeronautical Systems Division | 1 |
| (1 for Commander) | |
| USAF Flight Test Center | 1 |
| (1 for Commander) | |
| Army Aviation Systems Test Activity, Edwards AFB | 1 |
| (1 for Commanding Officer) | |
| Army Aviation Systems Command | 1 |
| (1 for Commanding General) | |
| General Dynamics, Convair Division | 1 |
| McDonnell Douglas Corp., St. Louis | 1 |
| Lockheed California Co. | 1 |
| Boeing Co. | 1 |
| LTV Aerospace Corp. | 1 |
| Rockwell International, Columbus | 1 |
| Rockwell International, Los Angeles | 1 |
| Fairchild Republic Corp. | 1 |

DISTRIBUTION LIST (Continued)

REPORT NO. NADC-81177-60
CONTRACT NO. N62269-81C-0395

| | No. of Copies |
|--|---------------|
| McDonnell Douglas Corp, Long Beach | 1 |
| Pratt & Whitney Aircraft | 1 |
| Northrop Corp. | 1 |
| Lockheed-Georgia Co. | 1 |
| Grumman Aerospace Corp. | 1 |
| General Dynamics Corp., Ft. Worth | 1 |
| Hughes Aircraft Co. | 1 |
| Defense Technical Information Center | 12 |
| Naval Air Development Center | |
| (3 for Code 8131) | |
| (1 for Code 605) | |
| (10 for Code 6053) | |

END

FILMED

3-83

DTIC